Physica Medica 73 (2020) 13–21

Contents lists available at ScienceDirect

Physica Medica

journal homepage: www.elsevier.com/locate/ejmp

Original paper

Determination of radiation dose and low-dose protocol for digital chest tomosynthesis using radiophotoluminescent (RPL) glass dosimeters

Sarawut Tongkum[a,b], Petcharleeya Suwanpradit[c], Sirachat Vidhyarkorn[b], Surachate Siripongsakun[d], Sornjarod Oonsiri[e], Yothin Rakvongthai[a,f,g], Kitiwat Khamwan[a,f,g,*]

[a] Medical Physics Graduate Program, Department of Radiology, Faculty of Medicine, Chulalongkorn University, Bangkok 10330, Thailand
[b] Department of Diagnostic and Interventional Radiology, Chulabhorn Hospital, Bangkok 10210, Thailand
[c] Division of Diagnostic Radiology, Department of Radiology, King Chulalongkorn Memorial Hospital, The Thai Red Cross Society, Bangkok 10330, Thailand
[d] Sonographer School, Faculty of Heath Science Technology, HRH Princess Chulabhorn College of Medical Science, Chulabhorn Royal Academy, Bangkok, Thailand
[e] Division of Radiation Oncology, Department of Radiology, King Chulalongkorn Memorial Hospital, The Thai Red Cross Society, Bangkok 10330, Thailand
[f] Division of Nuclear Medicine, Department of Radiology, Faculty of Medicine, Chulalongkorn University, Bangkok 10330, Thailand
[g] Chulalongkorn University Biomedical Imaging Group, Department of Radiology, Faculty of Medicine, Chulalongkorn University, Bangkok 10330, Thailand

ARTICLE INFO

Keywords:
Digital chest tomosynthesis
Entrance surface air kerma
Low-dose protocol
Radiophotoluminescent glass dosimeter
Pulmonary nodule detection

ABSTRACT

Purpose: This study aimed to determine a low-dose protocol for digital chest tomosynthesis (DTS).
Methods: Five simulated nodules with a CT number of approximately 100 HU with size diameter of 3, 5, 8, 10, and 12 mm were inserted into an anthropomorphic chest phantom (N1 Lungman model), and then scanned by DTS system (Definium 8000) with varying tube voltage, copper filter thickness, and dose ratio. Three radiophotoluminescent (RPL) glass dosimeters, type GD-352 M with a dimension of 1.5 × 12 mm, were used to measure the entrance surface air kerma (ESAK) in each protocol. The effective dose (ED) was calculated using the recorded total dose-area-product (DAP). The signal-to-noise ratio (SNR) was determined for qualitative image quality evaluation. The image criteria and nodule detection capability were scored by two experienced radiologists. The selected low-dose protocol was further applied in a clinical study with 30 pulmonary nodule follow-up patients.
Results: The average ESAK obtained from the standard default protocol was 1.68 ± 0.15 mGy, while an ESAK of 0.47 ± 0.02 mGy was found for a low-dose protocol. The EDs for the default and low-dose protocols were 313.98 ± 0.72 µSv and 100.55 ± 0.28 µSv, respectively. There were small non-significant differences in the image criteria and nodule detection scoring between the low-dose and default protocols interpreted by two radiologists. The effective dose of 98.87 ± 0.08 µSv was obtained in clinical study after applying the low-dose protocol.
Conclusions: The low-dose protocol obtained in this study can substantially reduce radiation dose while preserving an acceptable image quality compared to the standard protocol.

1. Introduction

Recently, the World Health Organization (WHO) reported that cancer is the second leading cause of death of people below 70 y-old, accounting for 9.6 million deaths globally in 2018 [1]. Amongst these cancers, lung cancer ranks as the most common cause of cancer deaths at approximately 1.76 million (18.4%) deaths according to the International Agency for Research on Cancer (IARC) report [2–4]. Given that most lung cancers are asymptomatic until later stages, the early detection of lung cancer by other means would increase the patient's survival rate. Although advance in diagnostic radiology technology have increased, chest radiography is still the most commonly used method for pulmonary disease screening. However, pulmonary lesions can be missed due to the limitations of chest radiography, since it projects the three-dimensional chest anatomy and pulmonary lesions onto a two-dimensional radiograph image, resulting in the overlapping of internal organ structures. Computed tomography (CT) is an advanced imaging modality showing a high sensitivity for nodule detection. Consequently, it became the gold standard for the detection of pulmonary abnormalities and lung carcinoma [5]. This modality, however, contributes a much higher radiation dose and higher cost compared to conventional chest radiography [6].

* Corresponding author at: Division of Nuclear Medicine, Department of Radiology, Faculty of Medicine, Chulalongkorn University and King Chulalongkorn Memorial Hospital, The Thai Red Cross Society, 1873 Rama IV Road, Pathumwan, Bangkok 10330, Thailand.
E-mail address: kitiwat.k@chula.ac.th (K. Khamwan).

https://doi.org/10.1016/j.ejmp.2020.03.024
Received 7 December 2019; Received in revised form 7 February 2020; Accepted 29 March 2020
1120-1797/

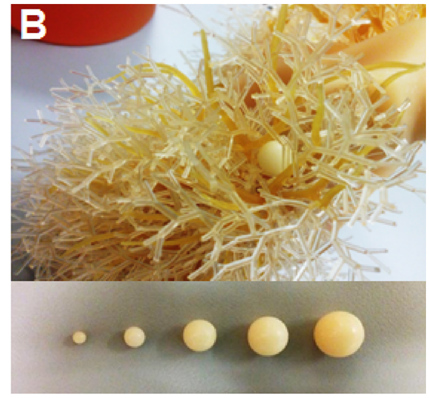

Fig. 1. (A) The multipurpose N1 lungman chest phantom and (B) five simulated nodules inserted in the lung field of the phantom.

Digital chest tomosynthesis (DTS) is an advanced acquisition technique using an x-ray flat panel detector, and has increasingly become of interest for lung cancer screening due to its ability in tomographic reconstruction to show anatomical structures at different depths from multi-sweep angle projection data. The modality allows the retrospective reconstruction of a number of planes from a series of low dose exposures acquired within a limited angular range. With these outstanding benefits for clinical applications, DTS has been recommended as an alternative investigation method in addition to chest radiography and CT scan. Furthermore, the greater diagnostic performance of DTS in detecting pulmonary nodules has been reported [7–9]. Although the radiologist has to spend more time interpreting the DTS images than a routine chest radiography, due to the multiple images per series, the overall interpretation time is still less than that for CT scans because of the significantly lower number of images to be evaluated [10]. Recent reports have shown that the DTS diagnosis time was lower than CT because of CT workload, and the diagnostic imaging costs were also decreased in patients with suspected pulmonary lesions after DTS implementation [5,7].

Although DTS has increasingly been accepted as an effective method for improving the detection of pulmonary abnormalities and nodules, the radiation dose is still substantially higher compared to chest radiography, with estimates of a three-fold higher radiation dose being exposed during DTS than by standard 2-view chest radiograph [7,11]. Based on previous studies, the range of the effective dose (ED) in the DTS between 100 and 300 μSv was obtained by changing the acquisition technique and parameters such as tube voltage, copper (Cu) filter thickness, and dose ratio [10,12]. The ED of 62 μSv using a low-dose setting protocol measured by the radiophotoluminescent (RPL) glass dosimeters in the anthropomorphic phantom was studied by Hwang et al [11]. Sabol JM revealed that an average ED in the DTS based on the Monte Carlo simulation was calculated to be 134 μSv using the tissue weighting factor according to the International Commission on Radiological Protection (ICRP) Publication 103 [13]. As such, it is of great interest to determine the appropriate parameters in DTS to reduce the radiation dose to the patient whilst maintaining a suitable image quality for interpretation. Consequently, this study aimed to (1) measure the radiation dose for DTS using radiophotoluminescent (RPL) glass dosimeters, and (2) determine a low-dose protocol and evaluate the image quality in a clinical study of patients being followed for pulmonary nodules. As a result, the low-dose protocol obtained from this study will likely improve the knowledge in diagnostic clinical dosimetry.

2. Methods

2.1. The DTS system and data acquisition

The DTS system (Definium 8000, GE Healthcare Waukesha WI) with VolumeRAD data acquisition technology at Department of Diagnostic and Interventional Radiology, Chulabhorn Hospital, Bangkok, Thailand, was used in this study. The flat-panel detector is based on an indirect conversion. For the DTS acquisition process, the detector position was fixed, while the x-ray tube moved continuously in a vertical plane in order to determine the exposure setting and patient positioning. After this scout image, the sweep angle was set at 30°with 60 low-dose projections through a tube angle from −15° to + 15° to acquire the data, resulting in a breath-hold acquisition time of 10 s [10,14]. Sixty reconstructed coronal images at various depths with a slice thickness of 4 mm without overlap and covering the entire chest region were obtained using the filter back-projection (FBP) algorithm. The default setting for the DTS in this study were 120 kVp, 125 mA, 2 ms (0.25 mAs per view), no additional copper (Cu) filter, and a dose ratio of 1:10 at 180 cm of source to image receptor distance (SID), while the scout image prior to the DTS was operated with an automatic exposure control (AEC).

2.2. Anthropomorphic N1 lungman chest phantom

The anthropomorphic chest phantom (N1 Lungman, Kyoto Kagaku, Kyoto, Japan), which is composed of a life-size main body with an inner component, including mediastinum, pulmonary vasculature and abdomen block (Fig. 1), was used to mimic the standard human chest. Soft-tissue materials and synthetic bones were made of polyurethane and epoxy resin, respectively. Synthetic nodules were simulated by polyurethane and hydroxyapatite spheres as solid types with a CT number approximately 100 Hounsfield Unit (HU) at 120 kVp. Five different sizes (inner diameter of 3, 5, 8, 10, and 12 mm) of synthetic nodules were inserted into the selected location of the lung filed of lungman phantom in order to simulate pulmonary lesions. The five locations and sizes of the simulated nodules were attached as follows: (1) 3-mm nodule at 2/3 peripheral of the right middle lobe, (2) 5-mm nodule at 1/3 peripheral of the left upper lobe, (3) 8-mm nodule at the right lower lobe, (4) 10-mm nodule at the peripheral of left lower lobe, and (5) 12-mm nodule at the right upper lobe.

2.3. Measurement of the entrance surface air kerma (ESAK)

In order to measure the ESAK in each protocol, the anthropomorphic phantom was positioned at the center of the x-ray beam and then scanned at a tube voltage of 100, 110, and 120 kVp, a Cu filter of 0.0, 0.1, 0.2, and 0.3 mm, and a dose ratio at 1:5, 1:8, and 1:10 for evaluating protocols of various doses. In this study, the AEC technique was used for the scout image to check the patient position. The DTS acquired data were then reconstructed using the filter back-projection (FBP) with a slice interval of 4 mm, resulting in 60 coronal section images that covered the entire chest of the phantom (or patient: next section). In total, 36 protocols, including the standard default protocol, were performed on the phantom. Each protocol was scanned three times. The standard default parameter setting at 120 kVp, no Cu filter and a 1:10 dose ratio was measured in order to compare the radiation dose and image quality with other protocols before considering the low-dose parameter. The artificial nodules of five different sizes were used for image quality assessment.

The radiophotoluminescent (RPL) glass dosimeters were used to measure the ESAK from the DTS in each protocol. Three RPL glass dosimeters (type GD-352 M, AGC Techno Glass Co., Ltd, Japan) with a dimension of 1.5 × 12 mm each were attached at the posterior surface of the N1 Lungman chest phantom, and the ESAK was measured at the center of the x-ray beam to represent the maximum x-ray intensity (T-7 level) [15]. The location of RPL glass dosimeters was consistently maintained for all measurements. The exposures were measured three times in each protocol in order to calculate the average dose value and uncertainty in terms of the standard deviation (SD). For the reading procedure, the dose value of the internal calibration glass, which was executed automatically, was used to determine the reading correction factor (in nanocoulombs, nC) for daily use condition. The coefficient of variation (CV) was also calculated in order to determine the reading reproducibility, where the CV must be within 5% or less at 100 µGy, and 2% or less at 1 mGy. The positioning of the phantom for measuring the ESAK and RPL glass dosimeter attachment is illustrated as in Fig. 2.

For RPL glass dosimeters used in this work, a tin filter in the capsule for GD-352 M was used in order to reduce the energy dependence effect purpose. Consequently, the RPL glass dosimeter type GD-352 M used in this study was suitable for measuring the radiation dose for low energy photons, such as in diagnostic radiology, whereas type GD-301 and GD-302 M without filters in the capsule are suitable to measure the dose of high energy photons, as in radiotherapy. However, in the process of dose readout, based on the dose values, the dose ranges were divided into the two categories of a low dose range from 10 µGy to 10 Gy, and a high dose range from 1 to 500 Gy) [16].

The dose-area-product (DAP, dGy/cm^2) was recorded from the displayed monitor in order to determine the effective dose (ED) in each protocol in addition to the ESAK. A conversion factor for tube voltage of 100, 110, and 120 kVp was applied as previously reported [17] to determine the EDs from the total registered DAP in VolumeRAD from the DTS examination using Eq. (1),

$$\mathrm{ED\,(mSv)} = \mathrm{Total\,DAP\,(Gy.cm^2)} \times \mathrm{conversion\,factor\,(mSv\,Gy^{-1}cm^{-2})} \tag{1}$$

2.4. Evaluation of image quality

2.4.1. Quantitative analysis

Image quality in terms of the quantitative analysis was evaluated by determining the signal-to-noise ratio (SNR) using the SYNAPSE software on the picture archiving and communication system (PACS) workstation. To compare the SNR at various protocols, the region of interest (ROI) was manually drawn on the simulated nodule size of 12 mm. The mean ± SD pixel intensity was recorded in order to evaluate the SNR in each protocol. The SNR was determined using the equation as followings:

$$\mathrm{SNR} = \frac{\textit{The mean pixel value of ROI in nodule}}{\textit{The standard deviation value of ROI in nodule}} \tag{2}$$

2.4.2. Qualitative analysis

The image quality criteria were evaluated independently by two radiologists who have a similar experienced in DTS interpretation (SV and SS). Currently, there is no specific protocol for DTS interpretation criteria, and so we used the European guidelines on quality criteria of chest radiography for DTS diagnostic radiographic images instead [18]. The acceptable overall scoring of the image criteria must be greater than three points. The image criteria and its scoring is shown in Table 1.

2.4.3. Nodule detection capability

Nodule detection was evaluated in accordance with the Fleischer Society Guideline, as reported by MacMahon et al [19,20]. The radiologists were blinded to the DTS scanning parameter techniques, and the images were analyzed in a randomized order by each reader. Nodule detection capability was graded on a PACS workstation (6 MP LCD color monitor) using a five-point Likert scale: where 1 denotes *poor* (visualize 12 mm with a sharp edge and partly visualize 10 mm); 2 denotes *fair* (visualize 10 mm with sharp edge and partly visualize 8 mm); 3 denotes *acceptable* (visualize clearly 8 with an edge and partly visualize 5 mm); 4 denotes very *good* (visualize clearly 5 mm, partly visualize 3 mm); and 5 denotes *excellent* (visualize all simulated nodules with a sharp edge). The acceptable score for nodule detection capability must be equal to or greater than three.

The low-dose protocol for DTS based on the anthropomorphic phantom in this work was selected by considering the acceptable image quality scoring and lung nodule detection capability interpreted by two radiologists as the priority. Then, the lowest reasonable radiation dose was considered thereafter.

3. Patient study

This study was approved by the institutional review board of the Faculty of Medicine, Chulalongkorn University, and the Chulabhorn Hospital (IRB No. 359/60). Thirty patients (15 males and 15 females) with a mean ± SD age of 60.4 ± 11.17 y-old (range 36 to 75 y-old) and body weight of 63.6 ± 10.39 kg undergoing DTS for pulmonary nodules follow-up at Chulabhorn Hospital were recruited for using the low-dose protocol derived from the phantom study. The inclusion criteria were patients who were requested for chest x-ray by the DTS technique, patient age > 35-y-old, chest thickness ranging between 15 and 25 cm, which was comparable to the anthropomorphic phantom chest thickness, high-risk smoker, family history of cancer, and

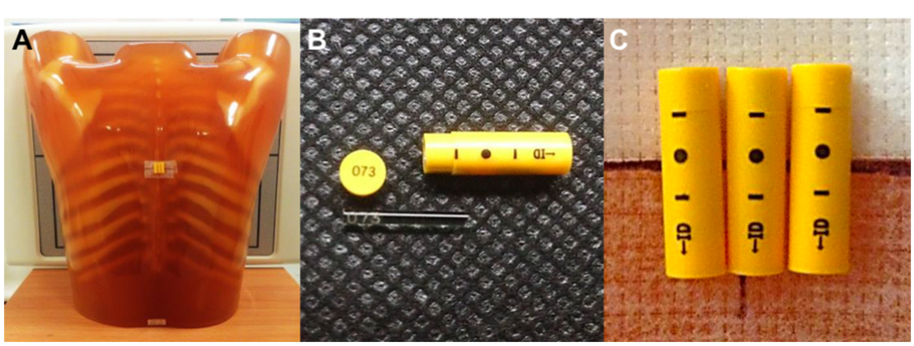

Fig. 2. Setting of the RPL glass dosimeters for measuring the ESAK in chest phantom study. (A) Positioning of the chest phantom during the radiation dose measurement. (B) Example of the RPL glass dosimeter. (C) Arrangement of the three dosimeters attached at the mid chest level of the phantom.

Table 1
Image criteria score for the DTS.

Item of image criteria score	Not fulfilled (0)	Partly fulfilled(0.5)	Fulfilled(1)
1. Visually sharp reproduction of the vascular pattern in the whole lung, particularly the peripheral vessels.			
2. Visually sharp reproduction of the trachea and proximal bronchi.			
3. Visually sharp reproduction of the borders of the heart and aorta.			
4. Visually sharp reproduction of the diaphragm and lateral costophrenic angles.			
5. Visualization of the retrocardiac lung and the mediastinum.			
6. Visualization of the spine through the heart shadow.			

*Criteria score > 3 (acceptable image quality)

pulmonary nodules follow-up. Emergency cases or unstable patients were excluded from this study. An informed consent form was obtained from each subject before the low-dose DTS examination. To evaluate the patient radiation dose obtained from a low-dose protocol, the conversion factor used in the phantom study [12,17] was multiplied by the recorded DAP value as shown in Eq. (1). The image quality after applying the low-dose protocol in patients was evaluated by radiologists using the image criteria scoring system in the same manner as in the phantom.

4. Results

Table 2 depicts the ESAK and ED measured from 36 DTS protocols in the anthropomorphic phantom study. The two lowest radiation dose protocols were found at 100 and 110 kVp, 1:5 dose ratio and a 0.3-mm Cu filter with an ESAK of 0.41 ± 0.01 mGy, and 0.47 ± 0.02 mGy, respectively. These were comparable to that previously reported for a low-dose setting of 0.31 mGy [11]. A trend of ESAK and ED decreasing with increasing Cu filter thickness over all ranges of tube voltages and dose ratios was observed. Conversely, and as expected, the ESAK and ED increased with an increasing dose ratio. The highest average SNR value (134.31 ± 1.30) for the artificial 12-mm nodule was found at 120 kVp, 1:5 dose ratio, and no additional Cu filter, with an ESAK of 1.48 ± 0.07 mGy. The low-dose parameter for the DTS in this study was selected at 110 kVp, 1:5 dose ratio, and 0.3-mm Cu filter as a better image quality and lower image noise, based on the image criteria score given by the two radiologists, was obtained compared to that at 100 kVp, with the same dose ratio and Cu filter. Thus, the radiation dose from the selected low-dose setting was dramatically lower (72%) than that from the standard default setting (120 kVp, 1:10 dose ratio, and no additional Cu filter). A strong positive linear relationship between the ESAK and recorded DAP value (R^2 = 0.952) was found as shown in Fig. 3. Figs. 4-6 depict a comparison of the image quality in nodule detection capability between the standard and low-dose protocols for detection of artificial nodules of 12, 8, and 3 mm diameter, respectively. There was no significant difference in the image quality and nodule detection capability between both reconstructed DTS image protocols.

In the clinical study, the average chest thickness of the 30 patients was 22.5 ± 1.69 cm, which was comparable to the chest thickness investigated in the anthropomorphic phantom (T-7 level of 21 cm). An average total DAP of 3.57 ± 0.08 dGy.cm^2 (range 3.42 – 3.72 dGy.cm^2) was obtained, giving an average ED of 0.099 ± 0.002 mSv (range 0.095 – 0.103 mSv). Fig. 7 shows the ED in each patient after applying the low-dose protocol in the clinical study of pulmonary nodule follow-up patients. The ED across the patients in this study were very consistent, since the AEC technique was used only for the scout image, while the mAs per projection (0.25 mAs per view) was similar in all patients in the DTS. Accordingly, the ED calculated from the total DAP value in the clinical study was obtained from the sum of values between the scout view and the DTS acquired in slightly different patient chest thickness.

For the image quality scoring, evaluated in the same manner as the anthropomorphic phantom, all of the low-dose DTS images were acceptable for interpretation with the image criteria score between 4 and 6 given by both radiologists (average image criteria score of 5.6 ± 0.7 and 5.8 ± 0.4 for the first and second radiologist, respectively). An example of the reconstructed DTS images using the low-dose setting for detection of pulmonary nodules compared to the previous standard default setting in the same patient is shown in Fig. 8. The low-dose protocol could detect the lesions at the right apex and right middle lobe of the lungs similar to the previous examination of the lung nodules follow-up patient. Fig. 9 depicts an example of magnified portion of the lesion at the middle lobe of lungs in pulmonary nodule follow-up patient using standard and low-dose setting protocols. It was found that the noise characteristics on the low-dose protocol image was slightly higher than the standard setting protocol.

5. Discussion

Although a CT scan can provide cross-sectional imaging for lung nodule detection and characterization, chest radiography still remains the mainstay for screening of many lung diseases. In addition, a CT scan requires a significantly greater radiation dose to the patient compared to conventional radiography. Developments in electronics and computer technology have led to advances in data acquisition and reconstruction utilizing a digital flat panel detector. The DTS has become as an alternative imaging modality offering a substantial improvement over conventional chest radiography for the detection of subtle lung disease due to its abilities to remove overlapping structures, enhance local tissue separation, and give depth information for the structure of interest [10,21]. However, the higher radiation dose compared to digital chest radiography should be considered when using this imaging modality [10].

In this study, low-dose protocols for DTS were investigated in order to reduce the radiation dose to patients while maintaining the image quality. The study was conducted in both an anthropomorphic phantom and then in clinical studies. The EDs for a DTS examination were previously reported to range from 0.1 to 0.3 mSv [10–13,22], which is close to the typical ED found in digital chest radiography. By optimizing the acquisition parameters, the ED could be reduced to 0.04 mSv without any significant decrease in the image quality [11]. Using a similar protocol to Hwang et al, the lowest ED in our study of 74 μSv were obtained at 100 kVp, dose ratio 1:5, and 0.3-mm Cu filter giving an 1.2-fold higher ED [11].

In a study of an anthropomorphic phantom, the ESAK measured from the standard default protocol (120 kVp, 1:10 dose ratio, and without a Cu filter) was 1.68 ± 0.15 mGy, while the low-dose protocol of this study (110 kVp, 1:5 dose ratio, and a 0.3-mm Cu filter) gave a 3.57-fold lower ESAK (0.47 ± 0.02 mGy). The ESAK of the default parameters was decreased by 52% when adding a 0.3-mm Cu filter, revealing its potential use in reducing the radiation dose to the patients [23,24]. This finding agrees with a previous report that a subjectively equivalent chest radiographic image quality was obtained with an approximately 30% dose reduction after the addition of a 0.3-mm Cu filter [25]. However, the ESAK obtained at a 1:5 dose ratio was not half of that obtained at a 1:10 dose ratio.

The EDs for the default and low-dose protocols in this study were

Table 2
The ESAK (mGy), ED (µSv), and SNR results for the 36 DTS protocols in phantom study.

Protocol No.	Dose ratio	Tube voltage (kVp)	Cu filter (mm)	ESAK (mGy)	ED (µSv)	SNR
1	1:5	100	0.0	1.07 ± 0.06	205.26 ± 0.83	133.68 ± 1.26
2			0.1	0.69 ± 0.02	127.13 ± 0.39	128.90 ± 1.47
3			0.2	0.51 ± 0.02	91.75 ± 0.26	127.42 ± 0.69
4			0.3	0.41 ± 0.01	74.36 ± 0.30	133.19 ± 1.20
5		110	0.0	1.26 ± 0.03	260.29 ± 0.42	132.38 ± 1.78
6			0.1	0.81 ± 0.01	167.68 ± 0.70	125.54 ± 1.72
7			0.2	0.60 ± 0.02	123.73 ± 0.42	127.53 ± 1.71
8*			0.3	0.47 ± 0.02	100.55 ± 0.28	128.58 ± 3.48
9		120	0.0	1.48 ± 0.07	314.26 ± 0.59	134.31 ± 1.30
10			0.1	0.94 ± 0.05	208.15 ± 0.44	122.75 ± 2.43
11			0.2	0.81 ± 0.04	156.28 ± 0.44	113.69 ± 3.30
12			0.3	0.72 ± 0.08	128.54 ± 0.28	115.75 ± 1.61
13	1:8	100	0.0	1.25 ± 0.10	205.00 ± 0.59	113.39 ± 0.50
14			0.1	0.88 ± 0.08	157.88 ± 0.15	129.79 ± 0.90
15			0.2	0.72 ± 0.05	113.34 ± 0.26	128.60 ± 1.39
16			0.3	0.69 ± 0.05	110.85 ± 0.30	133.93 ± 1.70
17		110	0.0	1.38 ± 0.06	260.66 ± 0.48	124.28 ± 1.99
18			0.1	0.80 ± 0.03	167.59 ± 0.28	131.37 ± 2.86
19			0.2	0.73 ± 0.04	123.45 ± 0.16	132.63 ± 0.70
20			0.3	0.70 ± 0.06	124.83 ± 0.16	122.74 ± 2.42
21		120	0.0	1.50 ± 0.05	314.55 ± 0.34	119.20 ± 1.05
22			0.1	1.12 ± 0.08	208.15 ± 0.44	120.61 ± 2.38
23			0.2	0.73 ± 0.02	156.66 ± 0.16	110.22 ± 1.98
24			0.3	0.62 ± 0.01	128.63 ± 0.16	127.60 ± 1.49
25	1:10	100	0.0	1.61 ± 0.04	255.54 ± 0.15	120.35 ± 1.19
26			0.1	1.02 ± 0.05	192.84 ± 0.65	108.90 ± 1.96
27			0.2	0.92 ± 0.03	138.27 ± 0.45	129.47 ± 0.09
28			0.3	0.74 ± 0.02	135.01 ± 0.30	115.53 ± 0.86
29		110	0.0	1.63 ± 0.09	326.77 ± 0.32	122.99 ± 0.36
30			0.1	1.09 ± 0.14	209.32 ± 0.32	124.43 ± 1.89
31			0.2	0.90 ± 0.04	165.65 ± 0.64	118.20 ± 3.95
32			0.3	0.83 ± 0.08	152.63 ± 0.28	114.98 ± 1.38
33**		120	0.0	1.68 ± 0.15	313.98 ± 0.72	115.24 ± 2.03
34			0.1	0.99 ± 0.02	207.96 ± 0.59	118.07 ± 3.50
35			0.2	0.99 ± 0.07	182.69 ± 0.57	120.74 ± 1.93
36			0.3	0.81 ± 0.06	160.74 ± 0.00	116.62 ± 2.62

*the low-dose protocol.
**the standard setting protocol.

313.98 ± 0.72 and 100.55 ± 0.28 µSv, respectively. The dose ratio and tube voltage were slightly correlated with the total DAP value, since the AEC technique was only applied for the scout image to check the patient positioning. The purpose of AEC was to achieve an adequate image quality by maintaining a constant optical density, and so changing the exposure parameters slightly affected the SNR measurement. There were slight differences in the image criteria score and nodule detection between the low-dose and default protocols, as assessed visually by the two radiologists according to the European guidelines on quality criteria for diagnostic radiographic images and the Fleischner Society guidelines [18–20]. The European guidelines on image quality criteria scoring were applied due to the lack of specific standard protocols for interpretation of DTS images.

In the clinical study, an average effective dose of 98.87 ± 0.08 µSv

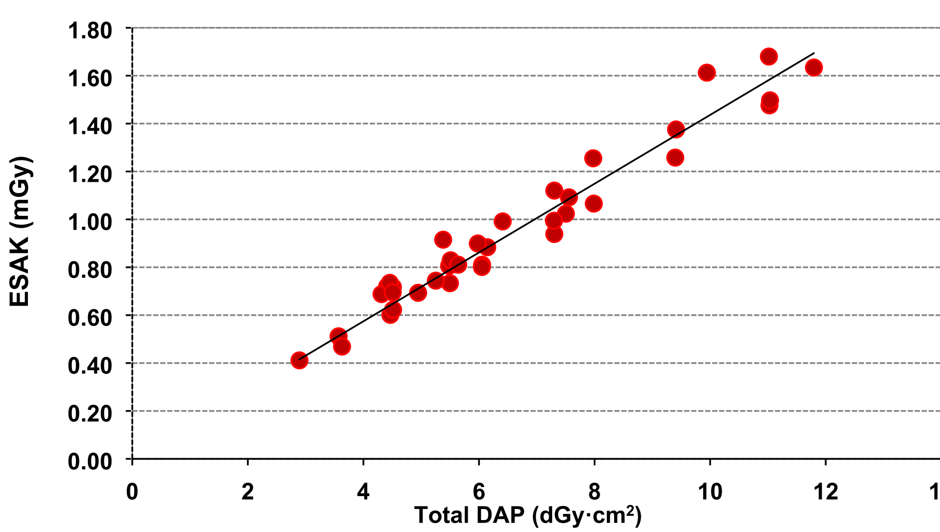

Fig. 3. Correlation between the ESAK (mGy) and DAP values (dGy.cm^2) obtained from the 36 protocols in the phantom study.

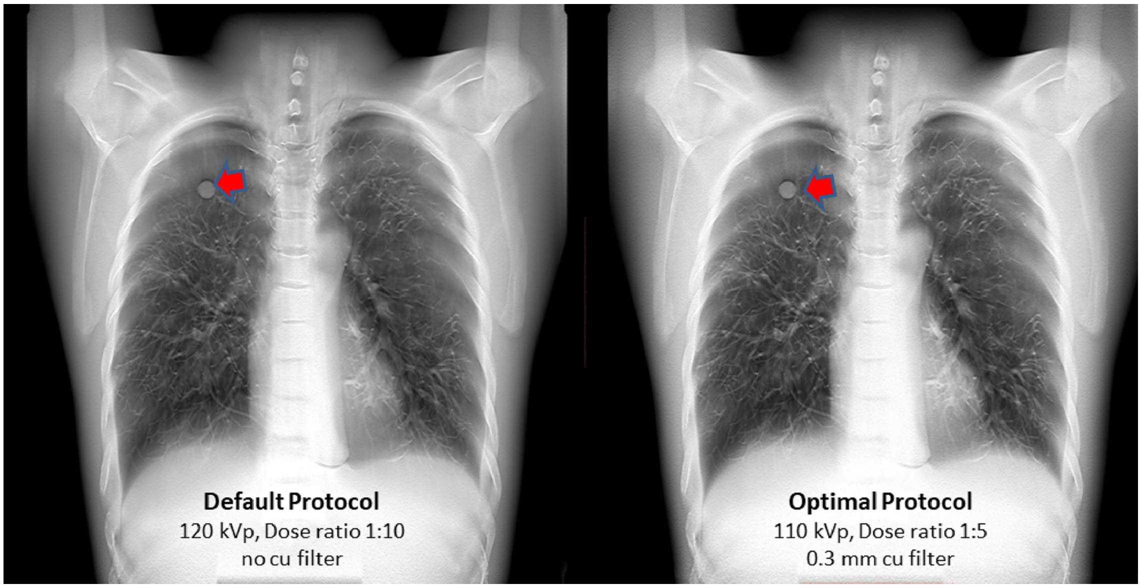

Fig. 4. Detection of the 12-mm diameter artificial nodule at the right upper lobe using the (Left) standard (default) protocol compared to the (Right) low-dose protocol.

was obtained after applying the low-dose protocol in 30 patients who were imaged for follow-up of pulmonary nodules. The image quality scores in all these patients were found to be acceptable for clinical interpretation by the two radiologists, where an image score of 6.0 was given for 19 (63%) and 24 (80%) cases by the first and second radiologist, respectively. This would indicate that the low-dose protocol investigated in this study was acceptable for clinical usefulness. However, the image quality score is dependent on patient stability as movement (either whole body or deep inspiration breath hold) during the breath-hold 10 s acquisition creates motion artifacts. Previously, Hwang et al described low-dose setting for DTS optimization resulted in a reduction of the radiation dose by 67% [11], which was achieved by keeping the dose per projection constant and reducing the number of projections. Those results are comparable with our study for the low-dose protocol resulting in a dose reduction of 72%, and could reduce the radiation risk of patients accordingly. However, the risk of health effects due to a very low level of radiation dose in diagnostic radiology should not be negligible, since it may cause the radiation-induced stochastic effect according to the linear no-threshold (LNT) model. In this effect, the severity of radiation damage is not related to the dose and the probability of occurrence increases with increasing radiation dose, e.g., development of cancer and secondary cancer. Therefore, increased awareness of risk of the exposure to ionizing radiation resulting in efforts to minimize radiation dose occurred during diagnostic imaging investigations [26–30].

The nodule detection capability in this study depended on the nodule size and the slice interval for image reconstruction, which agrees with the previous reports of a 53% and 71% detection sensitivity for 3–5 mm and 5–10 mm nodule sizes, respectively [8,31], and a sensitivity of 86% and nearly 100% for nodules of less than 4 mm and above 5 mm, respectively [32]. However, these results both showed a relatively low detection rate for nodules of less than 4 mm diameter, although in a clinical setting a nodule size of less than 4 mm can be negligible according to the Fleischner Society criteria. The

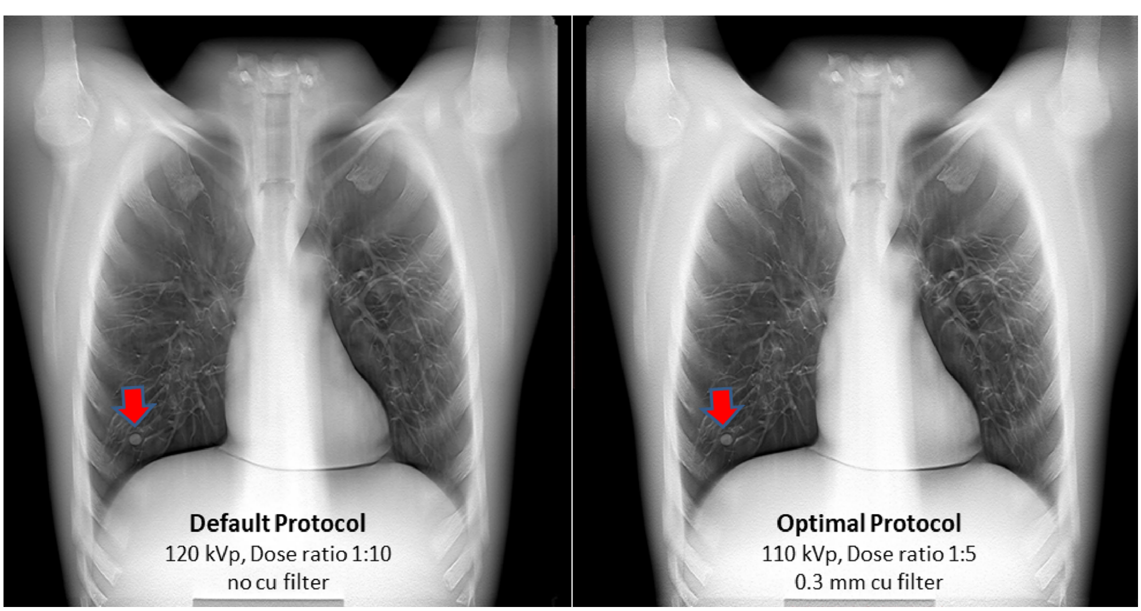

Fig. 5. Detection of the 8-mm diameter artificial nodule at the right lower lobe using the (Left) standard (default) protocol compared to the (Right) low-dose protocol.

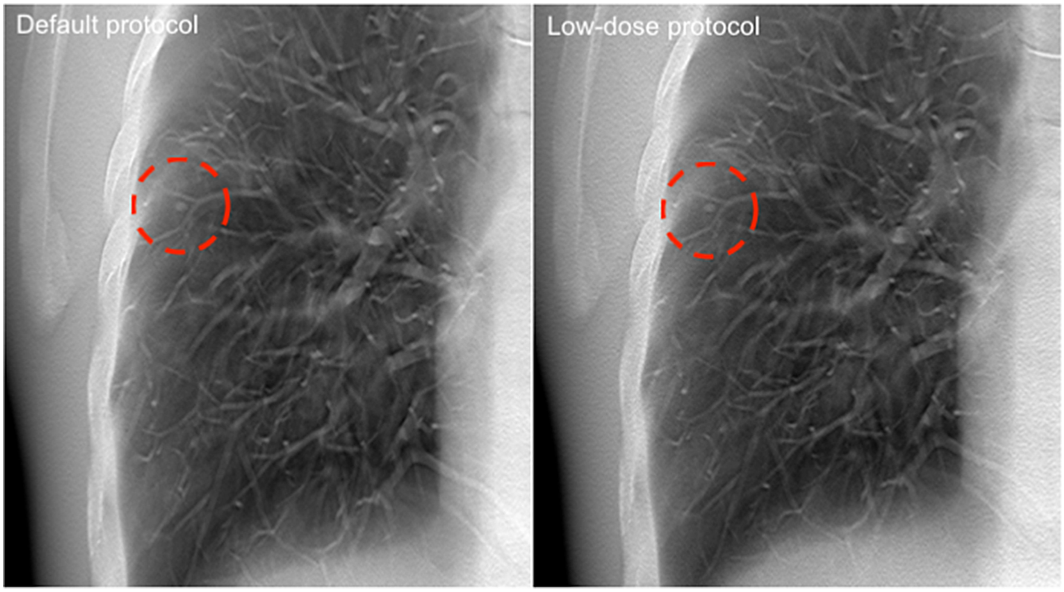

Fig. 6. Detection of the 3-mm diameter artificial nodule at the 2/3 in peripheral of the right middle lobe using the (Left) standard (default) protocol compared to the (Right) low-dose protocol.

implementation of DTS was proposed to be a potentially better option for high-risk patients, such as current or former smokers at risk for lung cancer and metastasis work-up patients [8]. This would maximize the chance for patient outcome improvement, while minimizing the examination cost, radiation dose, and workflow issues. Accordingly, we also suggested that the low-dose parameters setting in this study would be suitable for work-up patients.

6. Conclusions

This study successfully determined a low-dose protocol for chest x-ray using a DTS system. The protocol can substantially reduce radiation dose, while preserving the image quality, compared to the standard protocol, as demonstrated in both the phantom and clinical studies. Furthermore, the radiation dose was even lower than that for a low-dose CT chest scan for detecting pulmonary abnormalities and pulmonary nodules. The low-dose setting in this study is highly recommended for low risk patients such as non-smokers, young and pediatric patients, as well as the follow-up of lung nodule patients to minimize radiation dose.

Declaration of Competing Interest

The authors declare that they have no known competing financial interests or personal relationships that could have appeared to influence the work reported in this paper.

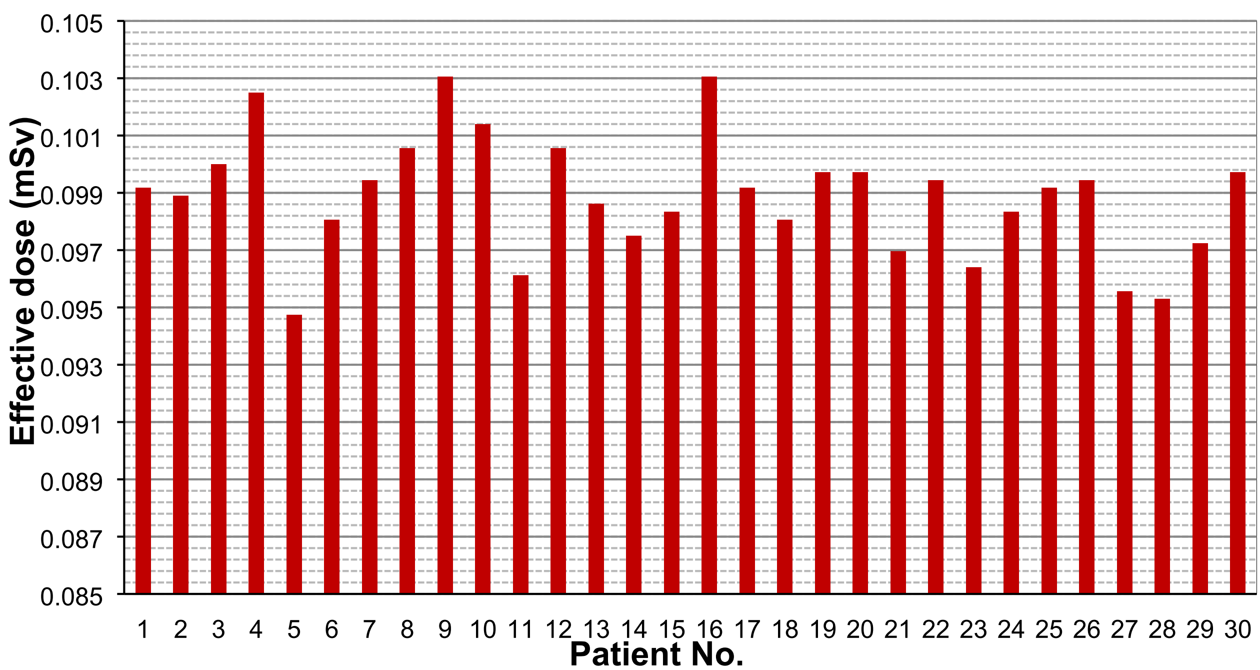

Fig. 7. The ED (mSv) obtained from 30 lung nodule follow-up patients.

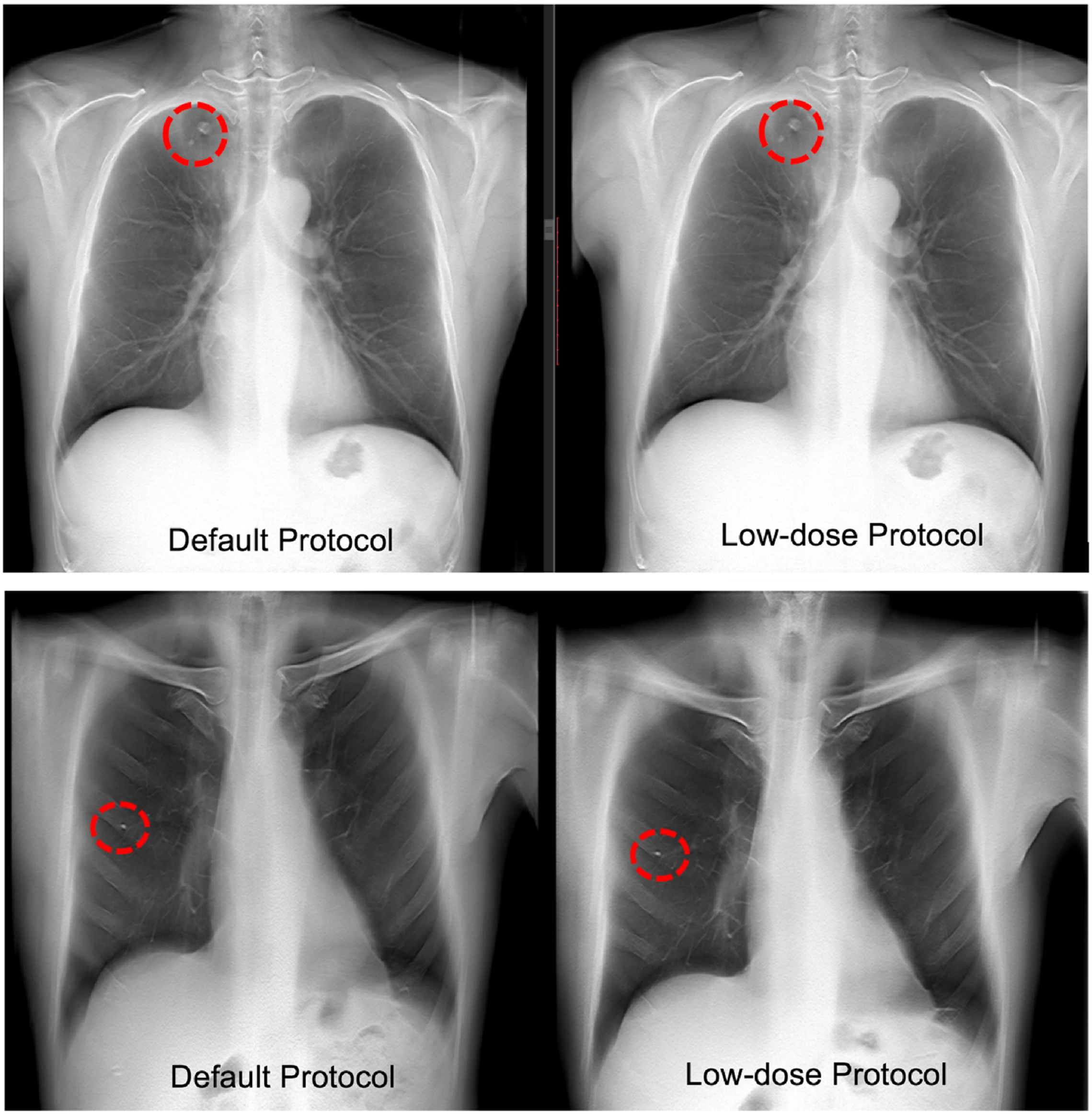

Fig. 8. Example of reconstructed DTS images of a lung nodule follow-up patient showing the lesions at (Upper) right lung apex and (Lower) right middle lobe using the (Left) standard default protocol and (Right) low-dose protocol.

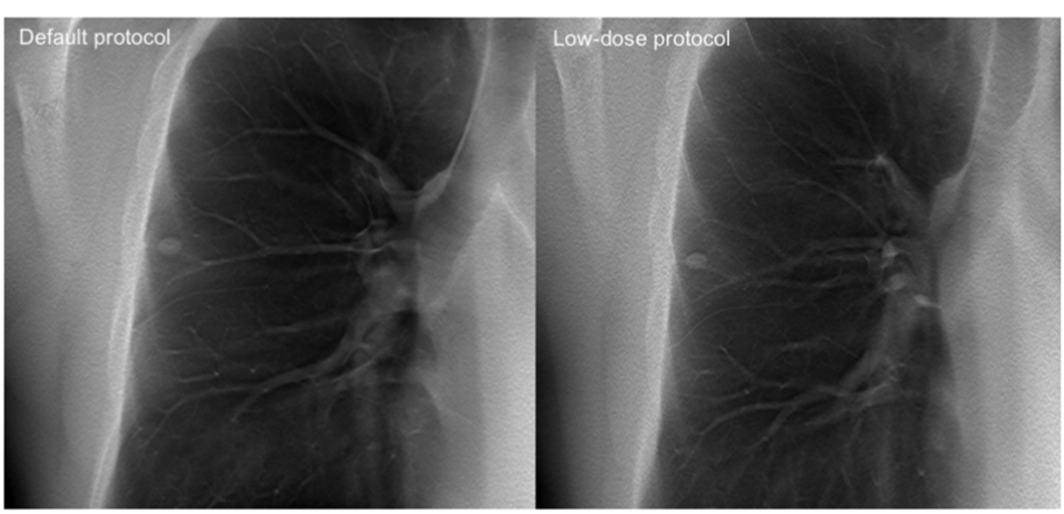

Fig. 9. Example of magnified portion images showing the lesion at the middle lobe of the lungs in pulmonary nodule follow-up patient using the (Left) standard setting protocol and (Right) low-dose protocol.

Acknowledgements

The authors sincerely thank to all radiological technologists and staffs who involved in this work at Department of Diagnostic and Interventional Radiology, Chulabhorn Hospital. We also thank medical physicists at Division of Radiation Oncology, King Chulalongkorn Memorial Hospital for helping in RPL glass dosimeter reading and calibration.

References

[1] World Health Organization. Global Health Observatory. Geneva: World Health Organization; 2018. who.int/gho/database/en/. Accessed January 27, 2020.
[2] Bray F, Ferlay J, Soerjomataram I, Siegel RL, Torre LA, Jemal A. Global cancer statistics 2018: GLOBOCAN estimates of incidence and mortality worldwide for 36 cancers in 185 countries. CA: a. Cancer J. Clin 2018;68(6):394–424.
[3] Siegel RL, Miller KD, Jemal A. Cancer statistics, 2019. CA: a Cancer Journal for Clinicians. 2019;69(1):7-34.
[4] Ferlay J, Colombet M, Soerjomataram I, Mathers C, Parkin D, Piñeros M, et al. Estimating the global cancer incidence and mortality in 2018: GLOBOCAN sources and methods. Int J Cancer 2019;144(8):1941–53.
[5] Quaia E, Grisi G, Baratella E, Cuttin R, Poillucci G, Kus S, et al. Diagnostic imaging costs before and after digital tomosynthesis implementation in patient management after detection of suspected thoracic lesions on chest radiography. Insights Imaging 2014;5(1):147–55.
[6] Kim JH, Lee KH, Kim K-T, Kim HJ, Ahn HS, Kim YJ, et al. Comparison of digital tomosynthesis and chest radiography for the detection of pulmonary nodules: systematic review and meta-analysis. Br J Radiol 2016;89(1068):20160421.
[7] Bertolaccini L, Viti A, Terzi A. Digital tomosynthesis in lung cancer: state of the art. Ann Transl Med 2015;3(10):139. https://doi.org/10.3978/j.issn.2305-5839.2015.06.03.
[8] Dobbins III JT, McAdams HP. Chest tomosynthesis: technical principles and clinical update. Eur J Radiol 2009;72(2):244–51.
[9] Dobbins III JT, McAdams HP, Sabol JM, Chakraborty DP, Kazerooni EA, Reddy GP, et al. Multi-institutional evaluation of digital tomosynthesis, dual-energy radiography, and conventional chest radiography for the detection and management of pulmonary nodules. Radiology 2017;282(1):236–50.
[10] Quaia E, Baratella E, Cernic S, Lorusso A, Casagrande F, Cioffi V, et al. Analysis of the impact of digital tomosynthesis on the radiological investigation of patients with suspected pulmonary lesions on chest radiography. Eur Radiol 2012;22(9):1912–22.
[11] Hwang HS, Chung MJ, Lee KS. Digital tomosynthesis of the chest: comparison of patient exposure dose and image quality between standard default setting and low dose setting. Korean J Radiol 2013;14(3):525–31.
[12] Båth M, Svalkvist A, von Wrangel A, Rismyhr-Olsson H, Cederblad Å. Effective dose to patients from chest examinations with tomosynthesis. Radiat Prot Dosim 2010;139(1–3):153–8.
[13] Sabol JM. A Monte Carlo estimation of effective dose in chest tomosynthesis. Med Phys 2009;36(12):5480–7.
[14] Machida H, Yuhara T, Mori T, Ueno E, Moribe Y, Sabol JM. Optimizing parameters for flat-panel detector digital tomosynthesis. Radiographics 2010;30(2):549–62.
[15] Alm-Carlsson G, Dance D, DeWerd L, Kramer H, Ng K, Pernicka F, et al. Dosimetry in diagnostic radiology: an International code of practice. Int Atomic Energy Agency Technical Reports Series. 2007;457.
[16] Huang DY, Hsu S-M. Radio-photoluminescence glass dosimeter (RPLGD). Advances in Cancer. Therapy: IntechOpen 2011.
[17] Svalkvist A, Månsson LG, Båth M. Monte Carlo simulations of the dosimetry of chest tomosynthesis. Radiat Prot Dosim 2010;139(1–3):144–52.
[18] Grewal R, Young N, Collins L, Karunaratne N, Sabharwal R. Digital chest radiography image quality assessment with dose reduction. Australas Phys Eng Sci Med 2012;35(1):71–80.
[19] MacMahon H, Austin JH, Gamsu G, Herold CJ, Jett JR, Naidich DP, et al. Guidelines for management of small pulmonary nodules detected on CT scans: a statement from the Fleischner Society. Radiology 2005;237(2):395–400.
[20] MacMahon H, Naidich DP, Goo JM, Lee KS, Leung AN, Mayo JR, et al. Guidelines for management of incidental pulmonary nodules detected on CT images: from the Fleischner Society 2017. Radiology 2017;284(1):228–43.
[21] Kumar SG, Garg MK, Khandelwal N, Gupta P, Gupta D, Aggarwal AN, et al. Role of digital tomosynthesis and dual energy subtraction digital radiography in detecting pulmonary nodules. Eur J Radiol 2015;84(7):1383–91.
[22] Söderman C, Asplund S, Johnsson ÅA, Vikgren J, Norrlund RR, Molnar D, et al. Image quality dependency on system configuration and tube voltage in chest tomosynthesis—a visual grading study using an anthropomorphic chest phantom. Med Phys 2015;42(3):1200–12.
[23] Söderman C, Johnsson ÅA, Vikgren J, Norrlund RR, Molnar D, Svalkvist A, et al. Evaluation of accuracy and precision of manual size measurements in chest tomosynthesis using simulated pulmonary nodules. Acad Radiol 2015;22(4):496–504.
[24] Jadidi M, Sundin A, Aspelin P, Båth M, Nyrén S. Evaluation of a new system for chest tomosynthesis: aspects of image quality of different protocols determined using an anthropomorphic phantom. The British Journal of Radiology. 2015;88(1053):20150057.
[25] Hamer OW, Sirlin CB, Strotzer M, Borisch I, Zorger N, Feuerbach S, et al. Chest radiography with a flat-panel detector: image quality with dose reduction after copper filtration. Radiology 2005;237(2):691–700.
[26] Tubiana M, Feinendegen LE, Yang C, Kaminski JM. The linear no-threshold relationship is inconsistent with radiation biologic and experimental data. Radiology 2009;251(1):13–22.
[27] Weber W, Zanzonico P. The controversial linear no-threshold model. J Nucl Med 2017;58(1):7–8.
[28] Vetter RJ. ICRP Publication 103. LWW: The Recommendations of the International Commission on Radiological Protection; 2008.
[29] Council NR. Health risks from exposure to low levels of ionizing radiation: BEIR VII phase 2. National Academies Press; 2006.
[30] O'Connor MK. Risk of low-dose radiation and the BEIR VII report: A critical review of what it does and doesn't say. Physica Med 2017;43:153–8.
[31] Dobbins JT, Samei E, Chotas HG, Warp RJ, Baydush AH, Floyd Jr CE, et al. Chest radiography: optimization of X-ray spectrum for cesium Iodide–amorphous silicon flat-panel detector. Radiology 2003;226(1):221–30.
[32] Vikgren J, Zachrisson S, Svalkvist A, AsA Johnsson, Boijsen M, Flinck A, et al. Comparison of chest tomosynthesis and chest radiography for detection of pulmonary nodules: human observer study of clinical cases. Radiology 2008;249(3):1034–41.